Hindawi
Advances in Polymer Technology
Volume 2020, Article ID 9408921, 9 pages
https://doi.org/10.1155/2020/9408921

Research Article

Adsorption of Chelerythrine from *Toddalia asiatica* (L.) Lam. by ZSM-5

Yunlong Liu, Jie Guo, Zhuobing Xiao, Dazhao Peng, and Ke Song

Key Laboratory of Forest Chemical Engineering of Hunan Province, Jishou University, Zhang Jiajie 427000, China

Correspondence should be addressed to Ke Song; kesong@jsu.edu.cn

Received 1 October 2019; Revised 25 November 2019; Accepted 27 November 2019; Published 3 January 2020

Guest Editor: Song Yang

Separation and purification of active components from biomass by inorganic materials during the pretreatment process of hydrothermal conversion are studied in this work. The batch experiment results show that an initial solution pH of 6 favors chelerythrine adsorption, and the optimum adsorbent dosage is 2.0 g. The adsorption mechanism of ZSM-5 for chelerythrine is investigated by adsorption kinetics, isotherm adsorption models, and thermodynamics analysis. The results show that the kinetics data fit the pseudo-second-order model well ($R^2 = 0.9991$), and the intraparticle diffusion model has 3 diffusion stages, preliminarily indicating that chemisorption plays a major role in the adsorption process, and the sorption mechanism includes intraparticle, external, and boundary diffusion. The adsorption isotherms agree well with the Langmuir model, indicating the occurrence of monolayer molecular adsorption during the adsorption process. Meanwhile, the maximum adsorption capacity is 2.327, 2.072, and 1.877 mg/g at different temperatures (288 K, 298 K, and 308 K), respectively. The thermodynamic data demonstrate that the adsorption process is exothermic and spontaneous in nature. These observed results clearly confirm that ZSM-5 has potential superior properties for the enrichment and purification of alkaloids during the pretreatment of biomass.

1. Introduction

Biomass, as a renewable carbohydrate found in nature, is a promising alternative to petroleum resources for the production of fuels, carbon-based chemicals, and materials [1, 2]. The pretreatment process of biomass before transformation is particularly important owing to the presence of various active components (e.g., flavonoids and alkaloids) in biomass. Therefore, isolating and purifying the active components from the pretreatment process of biomass are of great significance. In particular, Chelerythrine (CHE) is a common alkaloid that is found in the pretreatment process of *Toddalia asiatica* (L.) Lam., *Celandine*, *Macleaya cordata*, et al. As shown in Figure 1, the molecular formula and molecular weight of CHE are $C_{21}H_{18}NO_4^+$ and 348.37, respectively [3]. CHE has been widely used as an insecticide because it is harmful to the nerves and heart as well as it may cause paralysis, cardio-inhibitory activity, and even death. Moreover, CHE has shown favorable anti-inflammatory, antitumor, and antiplaque activity, as well as SH-enzyme inhibition [4–6]. The extraction of CHE from renewable biomass has received considerable attentions. Especially, *Toddalia asiatica* (L.) Lam. represents a better starting material to access CHE since *Toddalia asiatica* (L.) Lam. is easily available in nature and contains high amount of CHE. Therefore, it is very interesting to sustainably obtain CHE from *Toddalia asiatica* (L.) Lam. Furthermore, the residue after extraction can be used as a raw material for the production of value-added chemicals and biofuels, which enables the full utilization of *Toddalia asiatica* (L.) Lam. to be possible.

Many approaches, including resin adsorption [3, 7] and column chromatography [8–10], have been proposed to separate CHE from organic extracts. Although the two methods can achieve favorable CHE separation, the pretreatment and regeneration of the resin are complex and consume large quantities of reagents. Moreover, the high requirements for chromatographic equipment are not conducive to industrial applications. Therefore, developing a suitable carrier that is efficient and environmentally friendly for the enrichment and purification of alkaloids is necessary.

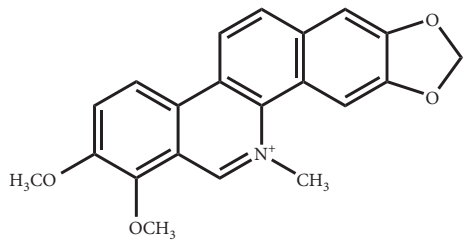

Figure 1: The molecular structure of chelerythrine.

Zeolite molecular sieves, as aluminosilicate crystals, are widely used in ion exchange [11], gas adsorption [12–14], and catalysis [15, 16] due to their regular structure, high surface area, and large inner pores. Since zeolites have holes connected by a plurality of pore canal structures with the same diameter, organic molecules with smaller size than the pore diameter can be adsorbed, while molecules with larger size than the pore diameter can be excluded, and then the organics can be separated. ZSM-5 is a typical representative of zeolite molecular sieves. It contains two types of channels: straight cylindrical channels with an oval cross section (channel size of 0.54 nm × 0.56 nm) and Z-shaped channels with an approximately circular cross section (channel size of 0.52 nm × 0.58 nm). Catalytic active centers and strong acid sites of ZSM-5 are concentrated at the intersections of the two channels [17–19]. In addition to its unique structural properties, the regeneration process of ZSM-5 is simple (calcinations in air for 4 h at the temperature of 873 K). Because of its mature technology and outstanding performance, ZSM-5 is widely used in the petrochemical industry [20], fine chemicals [21], environmental protection [22], and adsorption [23, 24].

The abundant acid sites and hydroxyl groups of ZSM-5 are expected to be obviously beneficial for adsorbing the target product. It is envisioned that ZSM-5 can efficiently purify target compounds from plant extracts on account of its unique structure. However, there are few reports on the application of molecular sieves in the field of separation and purification of plant active ingredients. Therefore, the adsorption of lycorine and galantamine by ZSM-5 molecular sieves from *Lycoris radiata* Herb. was reported in our previous study [24]; the results showed that the adsorption and desorption performance of lycorine and galantamine by molecular sieves was superior to those obtained using resin, which indicates that the application of molecular sieves in the separation and purification of active components from medicinal herb ingredients is promising. Therefore, to clarify the adsorption performance and mechanism of ZSM-5 towards active ingredients from plants, an alkaloid (CHE) was selected for use as a target and ZSM-5 was selected as an adsorbent. Batch experiments were used to study the optimal adsorption dose and initial solution pH. The adsorption kinetics, isotherms, and thermodynamics were investigated to explore the adsorption performance and mechanism of CHE on ZSM-5, and the technology described in this work is expected to be applied to isolate and purify the active ingredients from the pretreatment process of biomass.

2. Materials and Methods

2.1. Chemicals and Apparatus. Rhizomes of *Toddalia asiatica* (L.) Lam. were obtained from the planting base in Zhangjiajie. ZSM-5 (Na-type: Si/Al = 25, pore size 0.54 nm, surface area 380 m^2/g, and pore volume more than 0.21 cm^3/g) was purchased from Shanghai Saint Chemical Materials Co., Ltd., China. The ZSM-5 powder was placed in a muffle furnace, heated to 873 K at a heating rate of 2.4 K/min, and then calcined for 4 h at 873 K to remove organic impurities in the molecular sieves. A standard sample of CHE (≥98%, mass purity) was purchased from Shanghai Aladdin Biochemical Technology Co., Ltd., China, and chromatographic-grade acetonitrile was purchased from Fisher Scientific International Inc., America. Hydrochloric acid, phosphoric acid, methanol, and ammonia were purchased from Shanghai Titan Technology Co., Ltd., China; all these chemicals were analytical-grade reagents.

An Agilent-1260 high-performance liquid chromatograph from Agilent Co., Ltd. (America), equipped with a Waters C_{18} reverse-phase column (250 × 4.6 mm, 5 μm), was used for quantitative and qualitative analysis. An ultraviolet-visible spectrophotometer from SHIMADZU Co., Ltd., (Japan) equipped with a 1 cm cuvette was used for wavelength scanning. An FE20 laboratory pH meter from METTLER TOLEDO Co., Ltd., (Switzerland) was used for pH analysis.

2.2. Analytical Methodologies. A sample (2.0 g) of *Toddalia asiatica* (L.) Lam. powder was weighed accurately, infiltrated with 40 mL aqueous methanol (60%, v/v) for 30 min, and then ultrasonically extracted for 50 min at 333 K. The above process was repeated 3 times, and the extracted liquid was filtered. The filtrate was collected, concentrated to 20 mL under reduced pressure, and adjusted to pH = 6 with 1 mol/L HCl aqueous solution. The concentration of CHE in the extracts was analyzed by high-performance liquid chromatography (HPLC) under the following chromatographic conditions: a mixture of acetonitrile and 0.2% aqueous phosphoric acid (27 : 83 v/v) was used as the mobile phase with a flow rate of 1.0 mL/min, the temperature of the column was 303 K, and the UV detector was operated at 273 nm. The standard curves are shown in Figure 2. Prior to injection, the solutions were filtered through a 0.45 μm membrane; the injection volume was 20 μL.

2.3. Determination of Optimal Adsorption Capacity. The adsorption capacity is mainly determined by the initial solution pH and adsorbent dosage. Therefore, the adsorption of CHE was performed by using batch experiments with different initial solution pH values and adsorbent dosages. The pH was carefully adjusted by using 3.65 wt.% HCl and 3.5 wt.% NH_4OH to values in the range of 2 to 10. ZSM-5 with an adsorption dosage of 2.0~10.0 g was transferred to a conical flask containing 15 mL of extract. The two-factor sample solutions were vibrated for 24 h in a thermostatic shaker bath at a constant temperature of 288 K, and the

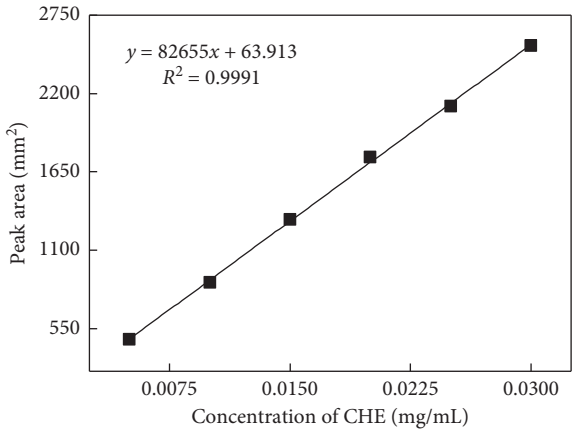

Figure 2: HPLC standard curve of CHE.

concentration of CHE in the solution was determined by using HPLC.

2.4. Adsorption Kinetics. A total of 2.0 g of ZSM-5 was added to 15 mL of solution at a concentration of 0.150 mg/mL, as described in Section 2.3, and the mixtures were stirred for 24 h by using a shaker at a constant temperature of 288 K. Samples were pipetted at certain intervals and determined by HPLC; the adsorption amount of ZSM-5 adsorbed at time t (q_t, mg/g) was calculated using the following equation:

$$q_t = \frac{(c_0 - c_t) \times V}{m}, \quad (1)$$

where c_0 and c_t (mg/mL) are the initial and time t concentrations of CHE in solution, respectively; V (mL) is the volume of the solution; and m (g) is the mass of ZSM-5.

2.5. Adsorption Isotherm. ZSM-5 (2.0 g) was added to 15 mL solutions containing CHE at concentrations from 0.050 to 0.500 mg/mL, and the mixtures were oscillated for 24 h until reaching adsorption equilibrium by using a shaker at constant temperatures of 288, 298, and 308 K. Known volumes of samples were pipetted and determined by HPLC. The equilibrium adsorption capacity (q_e, mg/g) of ZSM-5 was calculated using the following equation:

$$q_e = \frac{(c_0 - c_e) \times V}{m}, \quad (2)$$

where c_0, V, m, and q_e are as described above and c_e (mg/mL) is the equilibrium concentration of ZSM-5.

3. Results and Discussion

3.1. HPLC Analysis. The CHE contents of the standard solutions, extracts, and eluents were determined by HPLC. HPLC spectra of CHE are shown in Figure 3. From Figure 3(a), the standard solution has a characteristic peak at 11.83 min, while Figure 3(b) shows a characteristic peak at 10.11 min for the extracts. Figure 3(c) shows the peak of CHE at 10.53 min, which was determined using 80% ethanol solution with a pH of 2 to elute ZSM-5 at adsorption equilibrium. In addition, Figure 3(c) preliminarily proves that using ZSM-5 to enrich CHE from *Toddalia asiatica* (L.) Lam. is feasible.

3.2. Influence of pH. The hydrogen ion concentration is always considered one of the most important parameters in the adsorption process; it influences the surface binding sites or charges of the adsorbent and the degree of ionization/dissociation of CHE [25]. To study the influence of the initial solution pH on the adsorption of CHE, batch experiments at different pH values were carried out at 288 K with 15 mL of 0.150 mg/mL CHE and 2.0 g of adsorbent. Figure 4 shows that the adsorption capacity slightly increased with increasing initial pH and reached a maximum at pH 6. This trend occurred because at low pH, ether groups are protonated, which greatly weakens the binding capability between CHE and the active sites in molecular sieves. With further increases in pH, the adsorption capacity decreases sharply, mainly because of competitive adsorption; similar results have been shown in a previous study [26, 27].

3.3. Influence of Adsorbent Dosage. The influence of various amounts of ZSM-5 on adsorption capacity was studied in 15 mL of 0.15 mg/mL CHE methanol solution. The results are presented in Figure 5, which shows that the adsorption capacity decreases from 0.31 mg/g to 0.079 mg/g with an increase in adsorbent dosage from 2.0 g to 10.0 g due to the greater number of binding sites available. The adsorption rate increases substantially with increasing adsorbent dosage from 2.0 g to 6.0 g and increases slightly from 6.0 g to 10.0 g when CHE entirely occupies the available binding sites. Therefore, the amount of adsorbent was maintained at 2.0 g in the following experiments to optimize both the adsorption capacity and adsorption rate.

3.4. Adsorption Kinetics. The adsorption curves of ZSM-5 for CHE are plotted with adsorption capacity as the ordinate and time as the abscissa. As shown in Figure 6, the adsorption capacity increases rapidly during the initial 16 h and then gradually becomes flat until reaching equilibrium at 1.25 mg/g.

Adsorption kinetics models were used to illustrate the adsorption rate and mechanism of ZSM-5 [28]. Pseudo-first-order kinetics, pseudo-second-order kinetics, and intraparticle diffusion kinetics [29, 30] were used to evaluate the sorption kinetics; the equations are generally written as follows:

$$\ln(q_e - q_t) = \ln q_e - k_1 t,$$

$$\frac{t}{q_t} = \frac{t}{q_e} + \frac{1}{k_2 q_e^2}, \quad (3)$$

$$q_t = k_p t^{0.5} + C,$$

where k_1 (min^{-1}), k_2 ($\text{g}\cdot\text{mg}^{-1}\cdot\text{min}^{-1}$), and k_p ($\text{g}\cdot\text{mg}^{-1}\cdot\text{min}^{-1/2}$) are the pseudo-first-order kinetics, pseudo-second-order kinetics, and intraparticle diffusion kinetics rate constants of

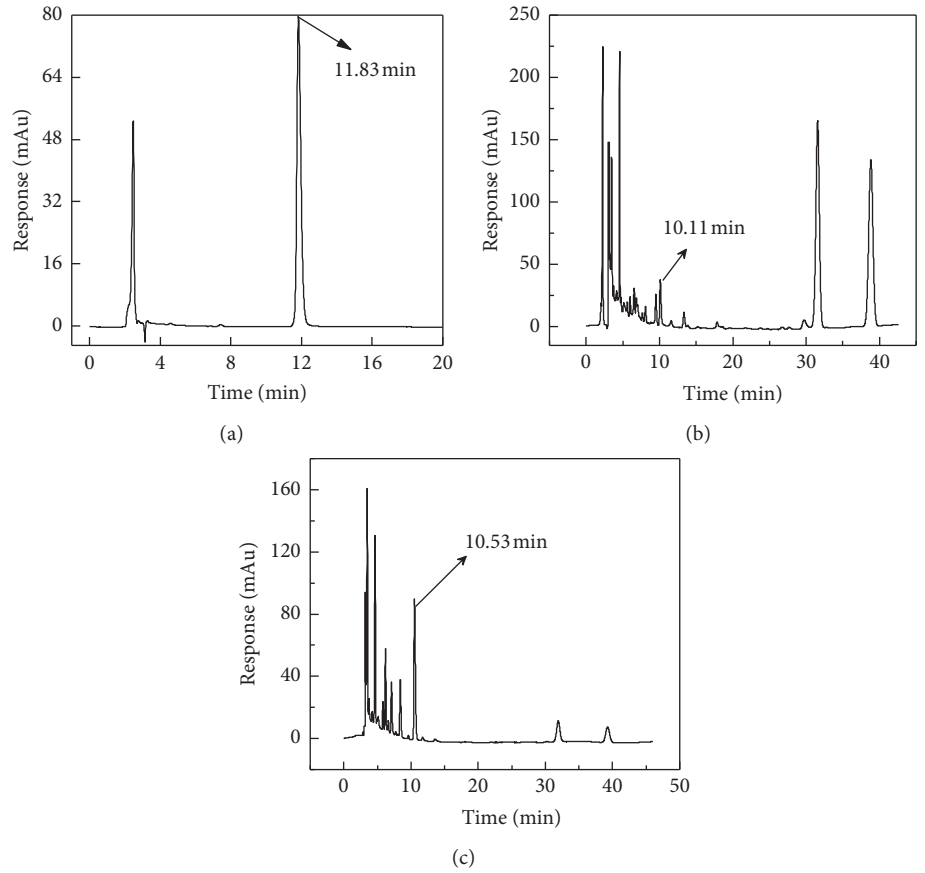

Figure 3: HPLC chromatograms of standard substance (a), extracts (b), and eluents (c).

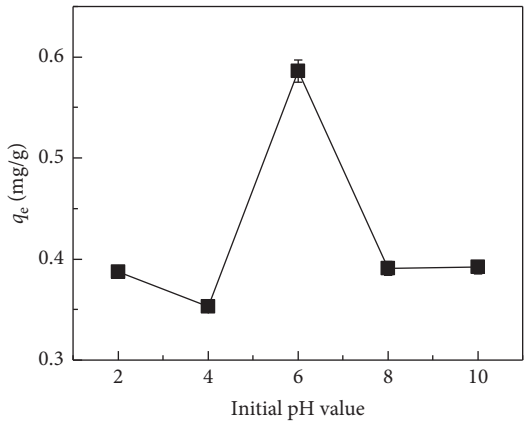

Figure 4: Influence of initial pH on adsorption capacity.

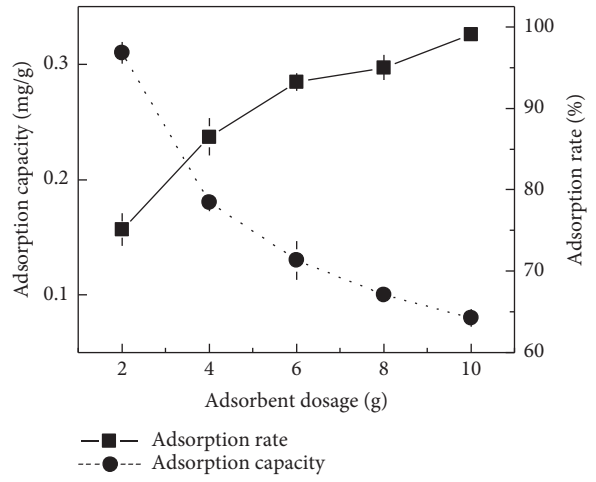

Figure 5: Effect of adsorbent dosage on adsorption capacity and adsorption rate.

adsorption, respectively; q_e (mg/g) is the equilibrium adsorption capacity; q_t (mg/g) is the amount of CHE adsorbed at time t; and C is the constant of adsorption.

According to the kinetics equations, the pseudo-first order, pseudo-second order and intraparticle diffusion kinetics curves are given by $\ln(q_e - q_t) \sim t$, $t/q_t \sim t$, and $q_t \sim t^{0.5}$, respectively. The fitting curves of the three kinetics models and their parameters are given in Figure 7 and Table 1, respectively. From Figure 7(a) and Table 1, the CHE adsorption data fit well with the pseudo-second-order kinetics model, as indicated by the high correlation ($R^2 = 0.9991$). This result indicates that chemisorption plays a major role in the adsorption process. From the fitting curve of the particle diffusion model in Figure 7(b), three stages exist during the diffusion of CHE to ZSM-5. k_{p1}, k_{p2}, and k_{p3}, which express the diffusion rates of the different stages in the adsorption process, are shown in Table 2 and follow the order

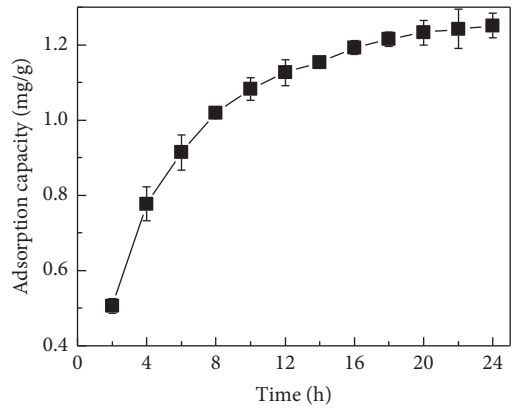

Figure 6: Adsorption kinetics curve.

$k_{p1} > k_{p2} > k_{p3}$. The first steeply sloped period is a rapid stage during which a large amount of CHE is rapidly adsorbed by the exterior surface of the molecular sieves. When the adsorption on the exterior surface reaches saturation, CHE molecules enter the pores of the adsorbent and are adsorbed by the interior surface of the molecular sieves. As the CHE molecules enter the pores, the diffusion resistance increases, which leads to a decrease in the diffusion rate. With the rapid decrease in CHE concentration, the intraparticle diffusion rate gradually falls and finally reaches equilibrium; therefore, the changes in k_{p1}, k_{p2}, and k_{p3} could be attributed to the different adsorption behaviors in the exterior surface adsorption stage, in the interior surface adsorption stage, and at equilibrium, respectively. The same result was obtained in a previous study [31]. In general, if the plot of q_t against $t^{1/2}$ gives a straight line and crosses the origin, intraparticle diffusion is the only rate-controlling step in the adsorption process. As shown in Figure 7(b), three straight lines were obtained, suggesting that intraparticle diffusion plays a major role but is not the only rate-controlling step in the adsorption process: external diffusion and boundary diffusion also influence the process.

3.5. Adsorption Isotherm. Adsorption isotherms are important for determining the adsorption behavior of an adsorbent. To simulate the adsorption behavior of molecular sieves for CHE, the adsorption curves of CHE on molecular sieves at different temperatures and solution concentrations were investigated. Figure 8 shows that the adsorption capacity increases with increasing solution concentration at a pH of 6, indicating that a high CHE concentration in solution is beneficial for adsorption by molecular sieves. Moreover, the results demonstrate that the molecular sieves show high affinity at lower temperatures.

To verify the adsorption process and clearly investigate the mechanism of adsorption, the Langmuir and Freundlich isotherms were applied to fit the experimental data in this study. The Langmuir isotherm model is based on the assumption that monolayer adsorption takes place onto a completely homogeneous surface that contains a limited number of active sites. The Freundlich isotherm is an empirical equation that describes adsorption onto a heterogeneous surface through a multilayer adsorption mechanism, and the sites on the surface have different binding energies [32]. The linear forms of the Freundlich and Langmuir adsorption isotherm equations are given as follows:

$$\ln q_e = \ln K_F + \frac{1}{n}\ln c_e,$$
$$\frac{1}{q_e} = \frac{1}{q_m} + \frac{1}{q_m K_L c_e}, \tag{4}$$

where q_e (mg/g) and q_m (mg/g) are the equilibrium and maximum adsorption capacity of CHE adsorbed by the molecular sieve, respectively; c_e (mg/mL) is the equilibrium concentration in solution; K_L (L/mg) and K_F (dm^3/mg) are the Langmuir and Freundlich adsorption constants, respectively; and n is the Freundlich constant, which is temperature-dependent.

The fitting parameters were calculated by linear plotting and are shown in Table 3. The constants n and K_F were calculated from the slope and intercept, respectively, of $\ln q_e$ versus $\ln c_e$ from Figure 9(a). The values of q_m and K_L can be calculated from Figure 9(b), the linear plot of c_e/q_e versus c_e. To choose the best-fitting model, the correlation coefficient (R^2) was studied. Comparing the values of R^2 from Table 3, we can conclude that the Langmuir model fits well with the experimental data for CHE adsorption on molecular sieves, indicating that a monolayer adsorption process occurs. According to the best fitting of the Langmuir model, the maximum adsorption capacities of CHE at 288, 298, and 308 K are 2.327 mg/g, 2.072 mg/g, and 1.877 mg/g, respectively. Moreover, the separation factor or equilibrium parameter (R_L) is introduced to describe the favorability of the CHE adsorption process; the formula of R_L is shown as follows:

$$R_L = \frac{1}{1 + K_L c_0}, \tag{5}$$

where c_0 (mg/dm^3) is the initial concentration of CHE. The favorability of the adsorption process is based on the value of R_L and can be irreversible ($R_L = 0$), favorable ($0 < R_L < 1$), linear ($R_L = 1$), or unfavorable ($R_L > 1$) [33]. The values of R_L shown in Table 3 are all positive; thus, the adsorption of CHE is favorable.

3.6. Adsorption Thermodynamics. Because the adsorption isotherm fits well with the Langmuir isotherm model at 288, 298, and 308 K, the adsorption enthalpy (ΔH), adsorption entropy (ΔS), and adsorption free energy (ΔG) of CHE on the ZSM-5 molecular sieves can be calculated using the Langmuir constant of K_L based on the following equations [34]:

$$\Delta G = -RT\ln K_a,$$
$$\ln K_a = -\frac{\Delta H}{RT} + \frac{\Delta S}{R}, \tag{6}$$

where K_a (dimensionless) is the thermodynamic equilibrium constant (the K_a values were estimated from the parameters of the Langmuir model, as presented in previous literature

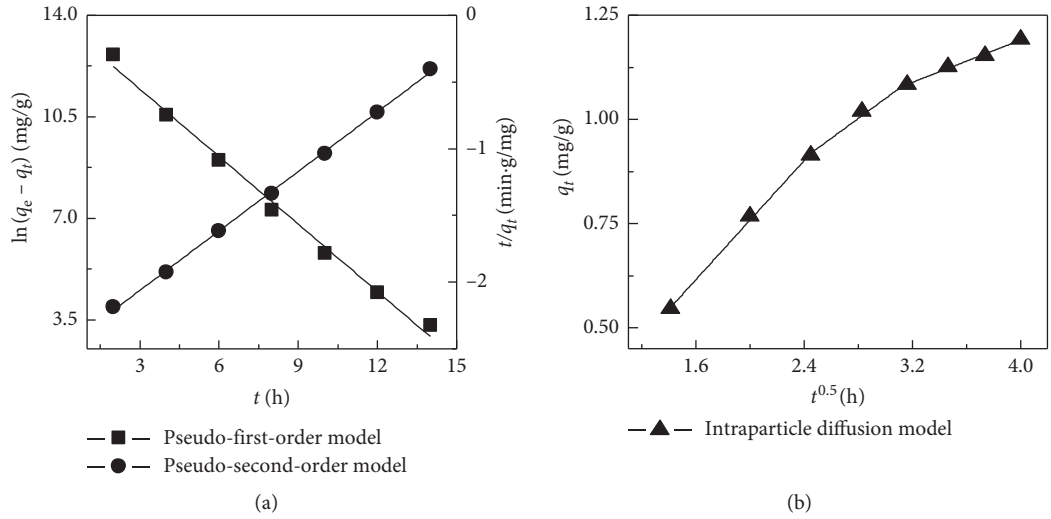

Figure 7: Fitting curves of various kinetics equations.

Table 1: Parameters of the pseudo-first-order and pseudo-second-order kinetics models.

Adsorbent	Pseudo-first-order kinetics model			Pseudo-second-order kinetics model		
	k_1 (min^{-1})	q_e (mg/g)	R^2	k_2 (g/mg·min)	q_e (mg/g)	R^2
CHE	0.0469	0.8446	0.9911	0.1959	1.4638	0.9991

Table 2: Fitting parameters of the intraparticle diffusion model.

Adsorbent	Intraparticle diffusion model					
	k_{p1} (g/mg $min^{1/2}$)	R^2	k_{p2} (g/mg $min^{1/2}$)	R^2	k_{p3} (g/mg $min^{1/2}$)	R^2
CHE	0.357	0.9969	0.238	0.9790	0.127	0.9910

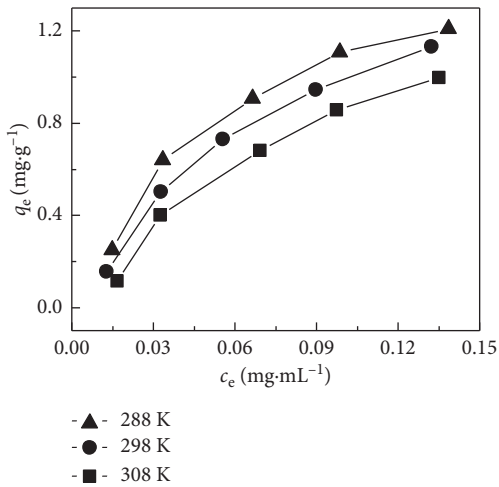

Figure 8: CHE adsorption isotherms of ZSM-5.

[35, 36]); R is the ideal gas constant, 8.314 J/(mol·K); and T is the absolute temperature (K). The values of ΔH and ΔS are calculated from the slope and the intercept of the linear plot of $\ln K_L$ versus $1/T$, respectively. The results are summarized in Table 4. The values of ΔG for CHE are negative, which implies that the adsorption of CHE by molecular sieves can happen spontaneously. Moreover, the values of ΔG increase gradually with decreasing adsorption temperature, which indicates that the lower the adsorption temperature is, the greater the affinity of binding sites and the more spontaneous the adsorption occurs. The negative value of ΔH implies that the adsorption of CHE is an exothermic process,

Table 3: Langmuir and Freundlich isotherm parameters of CHE on ZSM-5 at different temperatures.

Temperature (K)	Langmuir				Freundlich		
	Q_m (mg/g)	K_L (L/g)	R^2	R_L	K_F (dm^3/g)	$1/n$	R^2
288	2.327	13.905	0.9812	0.0024	3.836	0.556	0.9362
298	2.072	9.311	0.9872	0.0036	4.373	0.649	0.9579
308	1.877	5.758	0.9717	0.0051	4.636	0.744	0.9497

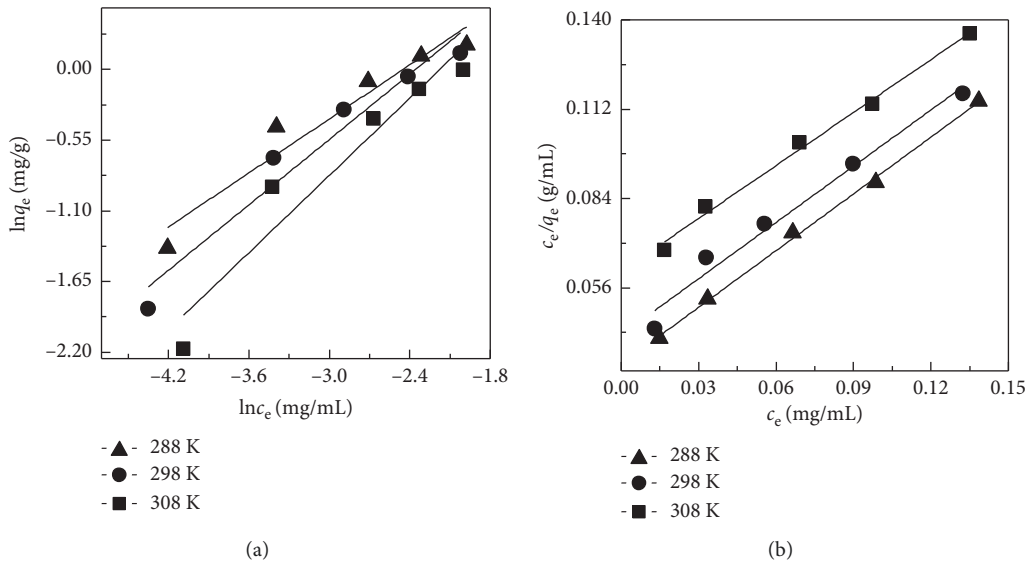

Figure 9: Fitting curves of the Freundlich model (a) and Langmuir model (b).

Table 4: Thermodynamic parameters for the adsorption of CHE on ZSM-5 at different temperatures.

Temperature (K)	ΔG (kJ/mol)	ΔH (kJ/mol)	ΔS (J/mol K)
288	−6.411		
298	−5.620	−67.232	−203.602
308	−4.556		

which demonstrates that decreasing the temperature is beneficial. The negative value of ΔS shows decreases in the degrees of freedom of the adsorbed species and the randomness at the solid/liquid interface.

4. Conclusions

This scientific study clearly suggests that ZSM-5 is suitable for adsorbing CHE from *Toddalia asiatica* (L.) Lam. Batch experiments revealed that the adsorption efficiency was affected by the solution pH, and the optimum initial solution pH was 6. The maximum adsorption capacity of CHE was found at a solid-liquid ratio of 2 : 15. The pseudo-second-order kinetics model and intraparticle diffusion model suitably describe the kinetics of the adsorption process, indicating that chemisorption plays a major role in the adsorption process and that intraparticle diffusion is not the only rate-controlling step in the adsorption process. The equilibrium adsorption data of CHE by ZSM-5 fit well with the Langmuir isotherm model, as indicated by the high correlation coefficients. The maximum adsorption capacities obtained from the Langmuir isotherm model in the temperature range of 288 K to 308 K are 2.327, 2.072, and 1.877 mg/g. The thermodynamic parameters show a favorable, spontaneous, and exothermic process in the adsorption of CHE by molecular sieves. In conclusion, as shown by the adsorption mechanism of the ZSM-5 molecular sieve for CHE, this material is thought to be a promising adsorbent for purifying alkaloids (especially quaternary ammonium alkaloids) from medicinal herbs. In addition, a technique for isolating active components from the pretreatment process of biomass is provided.

Data Availability

The data used to support the findings of this study are available from the corresponding author upon request.

Conflicts of Interest

The authors declare that there are no conflicts of interest regarding the publication of this paper.

Acknowledgments

This work was supported by the National Natural Science Foundation of China (no. 31560105), Zhangjiajie Science and Technology Development Project (no. 2015FJ2151), and

Graduate Student Scientific Research Innovation Projects of Jishou University (no. JGY201844).

References

[1] M. N. Catrinck, E. S. Ribeiro, R. S. Monteiro, R. M. Ribas, M. H. P. Barbosa, and R. F. Teofilo, "Direct conversion of glucose to 5-hydroxymethylfurfural using a mixture of niobic acid and niobium phosphate as a solid acid catalyst," *Fuel*, vol. 210, pp. 67–74, 2017.

[2] F. Parveen and S. Upadhyayula, "Efficient conversion of glucose to HMF using organocatalysts with dual acidic and basic functionalities-a mechanistic and experimental study," *Fuel Processing Technology*, vol. 162, pp. 30–36, 2017.

[3] Y. P. Shan, Y. H. Song, Y. Q. Liu, R. X. Liu, J. J. Du, and P. Zeng, "Adsorption of berberine by polymeric resin H103: kinetics and thermodynamics," *Environmental Earth Sciences*, vol. 73, no. 9, pp. 4989–4994, 2015.

[4] Y. Z. Zhu, Y. Y. Pan, G. B. Zhang et al., "Chelerythrine inhibits human hepatocellular carcinoma metastasis in vitro," *Biological & Pharmaceutical Bulletin*, vol. 41, no. 1, pp. 36–46, 2018.

[5] J. Jana, S. Mondal, P. Bhattacharjee et al., "Chelerythrine down regulates expression of VEGFA, BCL2 and KRAS by arresting G-Quadruplex structures at their promoter regions," *Scientific Reports*, vol. 7, no. 1, 2017.

[6] W. J. Lin, J. J. Huang, Z. W. Yuan, S. L. Feng, Y. Xie, and W. Z. Ma, "Protein kinase C inhibitor chelerythrine selectively inhibits proliferation of triple-negative breast cancer cells," *Scientific Reports*, vol. 7, no. 1, 2017.

[7] L. Y. Yao, Y. X. Zhu, C. Q. Liu, R. H. Jiao, Y. H. Lu, and R. X. Tan, "Preparative separation and purification of fumigaclavine C from fermented mycelia of Aspergillus fumigatus CY018 by macroporous adsorption resin," *Journal of Chromatography*, vol. 989, pp. 122–128, 2015.

[8] D. Castillo, M. Sauvain, M. Rivaud, and V. Jullian, "In vitro and in vivo activity of benzo c phenanthridines against leishmania amazonensis," *Planta Medica*, vol. 80, no. 11, pp. 902–906, 2014.

[9] A. Maurya and S. K. Srivastava, "Large-scale separation of clavine alkaloids from Ipomoea muricata by pH-zone-refining centrifugal partition chromatography," *Journal of Chromatography B*, vol. 877, no. 18-19, pp. 1732–1736, 2009.

[10] H. D. Luo, M. Peng, H. Y. Ye et al., "Predictable and linear scale-up of four phenolic alkaloids separation from the roots of *Menispermum dauricum* using high-performance counter-current chromatography," *Journal of Chromatography B*, vol. 878, no. 22, pp. 1929–1933, 2010.

[11] Y. H. Kwon, B. Min, S. W. Yang, D. Y. Koh, R. R. Bhave, and S. Nair, "Ion-Exchanged SAPO-34 membranes for krypton-xenon separation: control of permeation properties and fabrication of hollow fiber membranes," *Acs Applied Materials & Interfaces*, vol. 10, no. 7, pp. 6361–6368, 2018.

[12] Y. Shen, F. M. Wang, W. Liu, and X. B. Zhang, "The preparation of Fe^{3+} ion-exchanged mesopore containing ZSM-5 molecular sieves and its high catalytic activity in the hydroxylation of phenol," *Journal of Porous Materials*, vol. 25, no. 6, pp. 1587–1595, 2018.

[13] B. Li, X. L. Cui, D. O'Nolan et al., "An ideal molecular sieve for acetylene removal from ethylene with record selectivity and productivity," *Advanced Materials*, vol. 29, no. 47, 2017.

[14] L. Zhang, Y. Li, H. C. Zhou, and M. D. Chen, "Performance of 1,8-diazabicyclo [5.4.0] undec-7-ene-Modified SBA-15 for selective adsorption of CO2," *Energy & Fuels*, vol. 31, no. 3, pp. 3062–3068, 2017.

[15] X. T. Zhang, N. He, C. Y. Liu, and H. C. Guo, "Pt-Cu alloy nanoparticles encapsulated in silicalite-1 molecular sieve: coke-resistant catalyst for alkane dehydrogenation," *Catalysis Letters*, vol. 149, no. 4, pp. 974–984, 2019.

[16] L. D. Wang, S. Cui, Q. W. Li, J. Wang, and S. Liu, "Kinetics and mechanism of magnesium sulphite oxidation promoted by a novel cobalt-based molecular sieve catalyst," *Applied Catalysis A-General*, vol. 511, pp. 16–22, 2016.

[17] N. Ohnishi and K. Hiraga, "Slow-scan CCD camera analysis of electron diffraction and high-resolution micrographs of zeolite TPA/ZSM-5," *Journal of Electron Microscopy*, vol. 45, no. 1, pp. 85–92, 1996.

[18] S. Schallmoser, T. Ikuno, M. F. Wagenhofer et al., "Impact of the local environment of Bronsted acid sites in ZSM-5 on the catalytic activity in n-pentane cracking," *Journal of Catalysis*, vol. 316, pp. 93–102, 2014.

[19] R. Vonballmoos and W. M. Meier, "Zoned aluminium distribution in synthetic zeolite ZSM-5," *Nature*, vol. 289, no. 5800, pp. 782-783, 1981.

[20] X. H. Mu, D. Z. Wang, Y. R. Wang, M. Lin, S. B. Cheng, and X. T. Shu, "Nanosized molecular sieves as petroleum refining and petrochemical catalysts," *Chinese Journal of Catalysis*, vol. 34, no. 1, pp. 69–79, 2013.

[21] H. Belarbi, Z. Lounis, R. Hamacha, A. Bengueddach, and P. Trens, "Textural properties of ZSM-5 nanocrystals prepared in alkaline potassium fluoride medium," *Colloids and Surfaces A-Physicochemical and Engineering Aspects*, vol. 453, pp. 86–93, 2014.

[22] G. V. Briao, S. L. Jahn, E. L. Foletto, and G. L. Dotto, "Adsorption of crystal violet dye onto a mesoporous ZSM-5 zeolite synthetized using chitin as template," *Journal of Colloid and Interface Science*, vol. 508, pp. 313–322, 2017.

[23] H. Y. Liu, Z. K. Zhang, Y. Y. Xu, Y. F. Chen, and X. Li, "Adsorption-Oxidation reaction mechanism of NO on Na-ZSM-5 molecular sieves with a high Si/Al ratio at ambient temperature," *Chinese Journal of Catalysis*, vol. 31, no. 9-10, pp. 1233–1241, 2010.

[24] Y. L. Liu, S. Ke, Z. B. Xiao, and J. Guo, "Adsorption kinetics of lycorine and galantamine with molecular sieves ZSM-5," *Chemistry and Industry of Forest Products*, vol. 38, no. 3, pp. 122–128, 2018.

[25] Z. H. Chen, J. N. Zhang, J. W. Fu et al., "Adsorption of methylene blue onto poly (cyclotriphosphazene-co-4,4'-sulfonyldiphenol) nanotubes: kinetics, isotherm and thermodynamics analysis," *Journal of Hazardous Materials*, vol. 273, pp. 263–271, 2014.

[26] X. Z. Xu, S. X. Chen, and Q. H. Wu, "Surface molecular imprinting on polypropylene fibers for rhodamine B selective adsorption," *Journal of Colloid and Interface Science*, vol. 385, no. 1, pp. 193–201, 2012.

[27] S. Liao, W. Zhang, W. Long, D. Hou, X. C. Yang, and N. Tan, "Adsorption characteristics, recognition properties, and preliminary application of nordihydroguaiaretic acid molecularly imprinted polymers prepared by sol-gel surface imprinting technology," *Applied Surface Science*, vol. 364, pp. 579–588, 2016.

[28] L. Tang, G. D. Yang, G. M. Zeng et al., "Synergistic effect of iron doped ordered mesoporous carbon on adsorption-coupled reduction of hexavalent chromium and the relative mechanism study," *Chemical Engineering Journal*, vol. 239, pp. 114–122, 2014.

[29] M. Tanyol, N. Kavak, and T. Gülben, "Synthesis of poly (AN-co-VP)/zeolite composite and its application for the removal of brilliant green by adsorption process: kinetics, isotherms, and experimental design," *Advances in Polymer Technology*, vol. 2019, Article ID 8482975, 12 pages, 2019.

[30] J. S. He, A. A. Cui, F. Ni, S. H. Deng, F. Shen, and G. Yang, "A novel 3D yttrium based-graphene oxide-sodium alginate hydrogel for remarkable adsorption of fluoride from water," *Journal of Colloid and Interface Science*, vol. 531, pp. 37–46, 2018.

[31] W. J. Yang, P. Ding, L. Zhou, J. G. Yu, X. Q. Chen, and F. P. Jiao, "Preparation of diamine modified mesoporous silica on multi-walled carbon nanotubes for the adsorption of heavy metals in aqueous solution," *Applied Surface Science*, vol. 282, pp. 38–45, 2013.

[32] L. T. Tran, H. V. Tran, T. D. Le, G. L. Bach, and L. D. Tran, "Studying Ni (II) adsorption of magnetite/graphene oxide/chitosan nanocomposite," *Advances in Polymer Technology*, vol. 2019, Article ID 8124351, 9 pages, 2019.

[33] L. Tang, Y. Cai, G. D. Yang et al., "Cobalt nanoparticles-embedded magnetic ordered mesoporous carbon for highly effective adsorption of rhodamine B," *Applied Surface Science*, vol. 314, pp. 746–753, 2014.

[34] B. Erdem, A. Ozcan, and A. S. Ozcan, "Adsorption and solid phase extraction of 8-hydroxyquinoline from aqueous solutions by using natural bentonite," *Applied Surface Science*, vol. 256, no. 17, pp. 5422–5427, 2010.

[35] Y. Liu, "Is the free energy change of adsorption correctly calculated?," *Journal of Chemical and Engineering Data*, vol. 54, no. 7, pp. 1981–1985, 2009.

[36] X. X. Liu, W. P. Gong, J. Luo, C. T. Zou, Y. Yang, and S. J. Yang, "Selective adsorption of cationic dyes from aqueous solution by polyoxometalate-based metal-organic framework composite," *Applied Surface Science*, vol. 362, pp. 517–524, 2016.